

Plastic Limited Numerical Modelling on Contact Friction Effects of Steel–Concrete Connection for Composite Bridges

Original

Plastic Limited Numerical Modelling on Contact Friction Effects of Steel–Concrete Connection for Composite Bridges / Gosztola, D.; Cucuzza, R.; Szep, J.; Domaneschi, M.; Ghodousian, O.; Movahedi Rad, M.. - In: BUILDINGS. - ISSN 2075-5309. - 14:9(2024), pp. 1-19. [10.3390/buildings14092898]

Availability:

This version is available at: 11583/2993366 since: 2024-10-13T14:11:14Z

Publisher:

Multidisciplinary Digital Publishing Institute (MDPI)

Published

DOI:10.3390/buildings14092898

Terms of use:






This article is made available under terms and conditions as specified in the corresponding bibliographic description in the repository

Publisher copyright

(Article begins on next page)

Article

Plastic Limited Numerical Modelling on Contact Friction Effects of Steel–Concrete Connection for Composite Bridges

Dániel Gosztola ¹, Raffaele Cucuzza ², János Szép ¹, Marco Domaneschi ², Oveys Ghodousian ³
and Majid Movahedi Rad ^{1,*}

¹ Department of Structural and Geotechnical Engineering, Széchenyi István University, H-9026 Győr, Hungary; gosztola.daniel@sze.hu (D.G.); szepj@sze.hu (J.S.)

² Department of Structural, Building and Geotechnical Engineering, Politecnico Di Torino, Corso Duca degli Abruzzi, 24, 10129 Torino, Italy

³ Department of Civil Engineering, Takestan Branch, Islamic Azad University, Takestan 3481949479, Iran

* Correspondence: majidmr@sze.hu

Abstract: This research employs plastic limit analysis to examine load combinations, contact interactions, and friction effects on steel–concrete connections. A nonlinear finite element model was developed using ABAQUS 2021, incorporating the concrete damage plasticity model and contact friction interactions. The model's validity was confirmed through laboratory experiments. Results indicate that contact elements and friction between the top flange, concrete slab, and studs significantly influence structural behavior. Unlike conventional push-out tests, real deck–slab connections exhibit different load-displacement responses due to the self-weight and additional loads, such as vehicular traffic. Under horizontal loading, extensive failures with large deformations along the studs occur, while vertically compressive loads lead to failures around the connections.

Keywords: composite structures; friction effects; finite element modelling; push-out test; steel–concrete composite connection



Citation: Gosztola, D.; Cucuzza, R.; Szép, J.; Domaneschi, M.; Ghodousian, O.; Movahedi Rad, M. Plastic Limited Numerical Modelling on Contact Friction Effects of Steel–Concrete Connection for Composite Bridges. *Buildings* **2024**, *14*, 2898. <https://doi.org/10.3390/buildings14092898>

Academic Editor: Yonghui Wang

Received: 10 August 2024

Revised: 8 September 2024

Accepted: 10 September 2024

Published: 13 September 2024



Copyright: © 2024 by the authors. Licensee MDPI, Basel, Switzerland. This article is an open access article distributed under the terms and conditions of the Creative Commons Attribution (CC BY) license (<https://creativecommons.org/licenses/by/4.0/>).

1. Introduction

A paramount concern in steel–concrete composite systems centers on the shear connection between the different materials and solids. Early investigations into this research topic were primarily conducted through experiments, particularly push-out tests [1–4]. The headed stud connector swiftly gained popularity as a shear connector type, owing to its simplicity and expedited construction [5]. Numerous scientific experiments and thorough investigations have been conducted [6–8], contributing to an improved comprehension of the behavior of shear connections employing headed studs. Consequently, these findings have been incorporated into both practical applications and design codes, such as Eurocode [9]. During the parallel and subsequent periods, attention has diversified towards various research directions. In earlier times, scientific studies in this field were sometimes less numerous. However, in contemporary settings, a plethora of results are available concerning alternative connection types [10–13] and diverse applications [14–16].

Numerical approaches are taking on an increasingly significant role alongside and instead of experimental research. The common method is to develop a numerical model and verify its accuracy via a small-scale laboratory experiment, rather than conducting large-scale tests. Economic and sustainability factors aside, another benefit is that the numerical models may also serve for further research purposes. For instance, researchers have developed numerical models to analyze the performance of steel–concrete composite systems [17,18]. These models incorporate detailed representations of the connection elements, such as headed studs, and account for nonlinear material behavior. It is worth noting that while 3D finite element numerical models come with numerous advantages, their complexity and the multitude of parameters can lead to imprecise results across

various configurations. Therefore, the validation process through laboratory tests has become the standard approach in civil engineering, especially in the nonlinear modeling steel [19] and concrete [20,21].

Focusing on the problem of modeling shear connections in composite structures made of steel and concrete, this process can also be challenging because of the setting of many parameters. Researchers have evaluated several characteristics, including, for example, the contact and friction effects of steel–concrete composite actions. Oguejiofor [22] and Hosain [23] focused on comparison by conducting an analysis of shear and stud connectors push-out specimens utilizing these connectors. According to Jayas and Hosain, even at low load levels, there was concrete separation behind the shear connector [24]. Kim et al. [25] and El-lobody and Young [26] conducted studies on the behavior of headed studs in steel–concrete composite bridges which used profiled steel sheeting. Both studies considered the contact with separation between the shear connector and concrete, but they used different methodologies to address this issue. El-lobody and Young [26], and El-lobody and Lam [27] utilized a finite element (FE) code ABAQUS to conduct their research, utilizing a non-linear FE model with solid three-dimensional elements. They implemented contact separation on the stud shank surface that faces the load between the shear connector and the concrete in their modelling. Nguyen et al. [28] delved into the behavior of the steel–concrete composite connection, exploring various parameters such as stud diameter and concrete strength. Their investigation modeled the slab, beam, and stud partitions using eight-node brick elements with reduced integration stiffness (C3D8R) in ABAQUS. Mirza and Uy [29] concentrated on the combination of axial and shear loading of the steel studs. In their work, the steel flange and concrete slab elements were coupled.

Newer research on fatigue performance, such as the works on H-piles in jointless bridges by Karalar and Dicleli [30,31], sheds light on the effects of cyclic loading on structural fatigue and durability. These investigations have compared experimental findings with finite element simulations, focusing on how pile orientation and strain distribution influence fatigue life. Such studies underline the necessity of including dynamic loading conditions in finite element models to reflect real-world performance more accurately.

Guezouli and Lachal [32] investigated the effect of the friction coefficient on the load-slip behavior of steel–concrete composite specimens using a unique 2D nonlinear finite element model. This study also examined the distribution of internal stresses and deformations within the concrete slab. The results confirmed the important effect that contact components and friction play between the concrete slab and the studs as well as between the top flange and the concrete slab. However, authors pointed out that friction would probably be more significant in an actual steel–concrete composite structure that is subjected to the slab's weight and possible overload.

To find the static friction coefficient among cast-in-place concrete and rolled steel plates, Rabbat et al. [33] carried out an experiment study in their work, without the use of studs. They found that increasing vertical compressive stress leads to higher shear forces between the steel plate and concrete. Our study employs plastic limit analysis to investigate the impact of load combinations, contact interaction, and friction effects on steel–concrete connections, with a focus on validating the finite element model of the structural components based on experimental push-out test results. The aim is to gain a comprehensive understanding of the role played by contact and friction interactions in composite structures of steel–concrete materials under different horizontal and compression loads. Notably, the study reveals that the push-out test outcomes deviate from the real deck–slab connection.

This paper is structured as follows: Section 2 outlines the conducted experimental tests, while Section 3 is focused on preparing and validating FE modeling. Section 5 presents the plastic limit analysis. Section 6 provides a detailed analysis of the modeling approach for the deck slab-girder connection with the concrete slab under compression. In Section 7, the research outcomes and future developments are summarized.

2. Experimental Tests

Experimental tests were performed to assess the structural integrity and performance characteristics of the tested specimen, focusing on its response to the applied loads. Thus, the data obtained are used in the subsequent section for numerical modelling.

In addition to realistic specimen fabrication, the study includes comprehensive laboratory testing of material properties. The tensile and compressive characteristics of the concrete are precisely assessed, enhancing the accuracy of the finite element model and ensuring reliable experimental results.

These unique aspects of the experimental approach and modeling techniques collectively enhance the applicability and precision of the findings, offering valuable insights into the behavior of steel–concrete composite structures under realistic loading conditions.

2.1. Tested Specimen

Three push-out tests were conducted as depicted in Figure 1 using test specimens with geometric and material parameters derived from corresponding real bridge structures, consistently with prevailing practices in the domestic context. In the design and fabrication of the test specimens, meticulous attention was given to replicating real-world conditions. Throughout the research, the specimens were produced in collaboration with the largest bridge construction company in Hungary, facilitated through a Cooperative Doctoral Program. Ensuring the fidelity of the test specimens, we maintained consistency with actual bridge construction practices in terms of material, geometry, and fabrication of the steel girder. The quality, geometry, and type of studs, as well as the welding techniques, adhered to industry practice. Furthermore, the concrete utilized in the specimens was selected and applied with the same precision, methods, and conditions as those employed in bridge construction projects. This test was prepared according to the standard test outlined in Eurocode [9]. The loads were applied in load steps, and the testing closely followed the methodology given in the standard.



Figure 1. Test setup.

The model consists of two materials: concrete as well as steel, as illustrated in Figure 2. The concrete slab measures 700 mm in width and 300 mm in thickness, whereas the steel beam has a thickness of 16 mm. The rebar has a diameter of 12 mm, while the studs measure 125 mm in height and 22 mm in diameter.

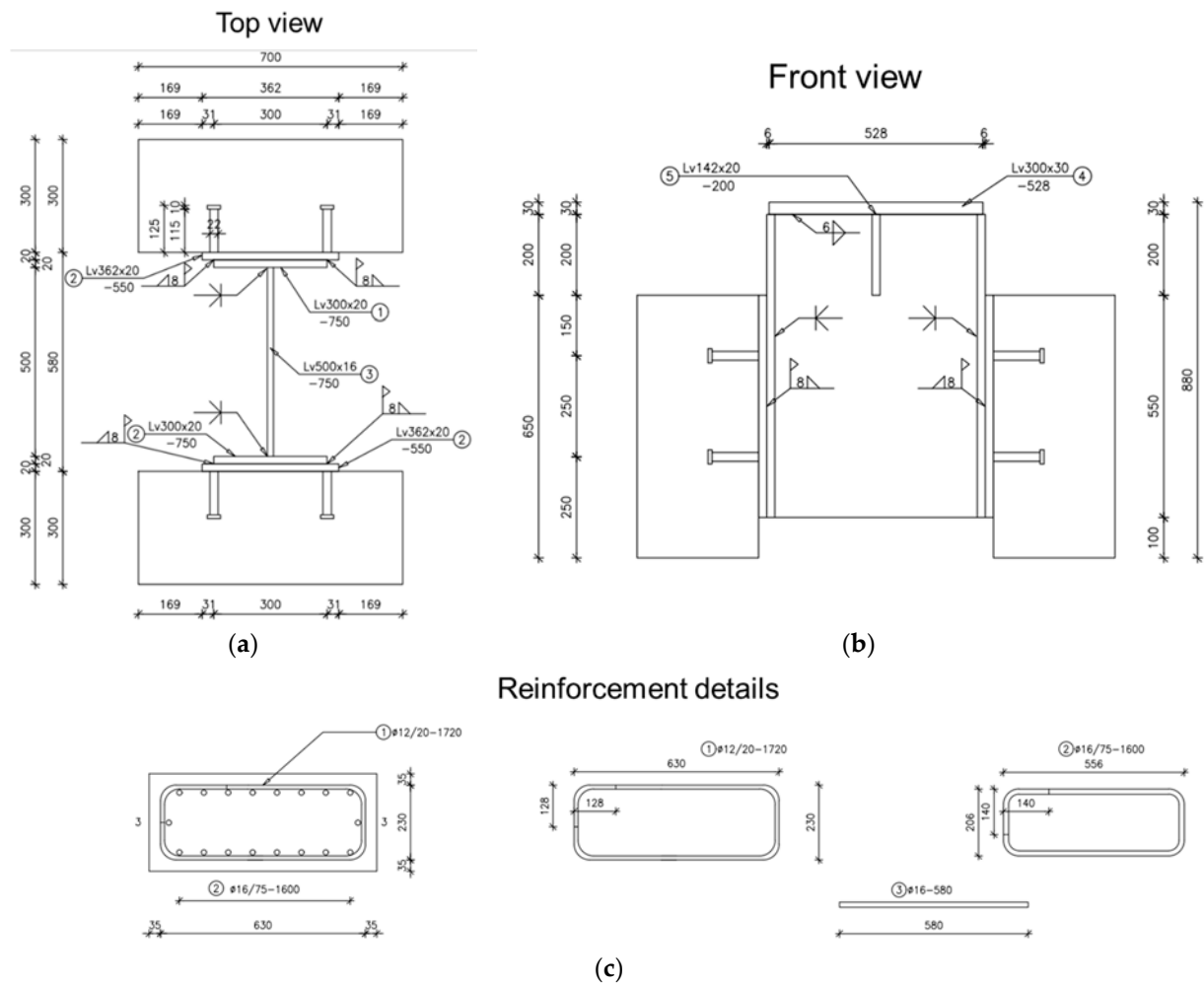


Figure 2. Specimen details: (a) Top view; (b) Front view; (c) Reinforcement details.

2.2. Material Properties

The composite steel–concrete model was experimentally evaluated in the laboratory of Széchenyi István University. The properties of the reinforcement steel bars are detailed in Table 1. Furthermore, laboratory experiments were conducted to determine the characteristics of the concrete. After a curing period of 28 days, four samples were prepared and assessed for each experiment. The experimental investigations were carried out within the laboratory setting to determine the average tensile and compressive strength of concrete, as illustrated in Figure 3.

Table 1. The considered material properties.

Material	Class	Ultimate Strength (f_u) [MPa]	Modulus of Elasticity (E) [MPa]	Yield Strength (f_y) [MPa]
Reinforcing steel	B500B	550	200,000	500
Structural Steel	S355J2	563	210,000	500
Studs	SD1 (S235J2 + C470)	534	210,000	509

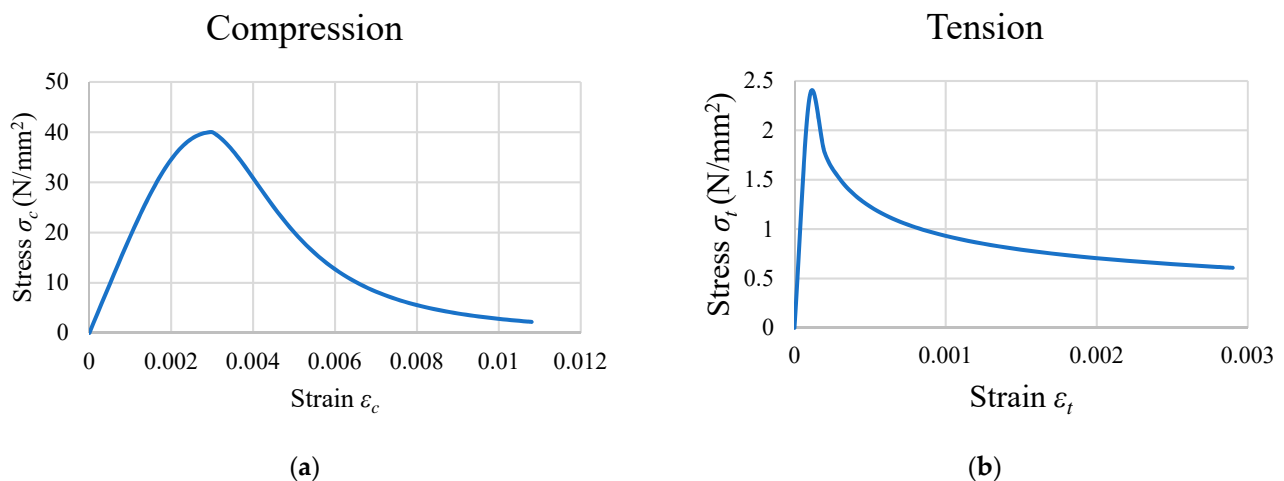


Figure 3. Properties of concrete. (a) Compression; (b) Tension.

3. Finite Element Modelling

Finite element modeling employed advanced features such as geometric nonlinearity, a bilinear isotropic hardening model for steel studs, and a Concrete Damage Plasticity (CDP) model for concrete. These elements enable a detailed simulation of complex stress states, large deformations, and failure mechanisms, thereby providing a thorough analysis of the composite structure's behavior. Furthermore, the mesh sensitivity analysis conducted was extensive, optimizing both accuracy and computational efficiency. Finer mesh sizes were applied in regions of maximum stress to ensure the precision of the numerical results, contributing to the overall reliability of the model.

The push-out specimen comprises four distinct components: steel reinforcements, steel beam, steel studs, and concrete materials, as depicted comprehensively in Figure 4. Each component was modeled as an individual part within the finite element model. The concrete slab section was modeled using the C3D8R solid element provided by the ABAQUS library. This element type features an eight-node brick configuration with reduced integration stiffness, which has been widely validated for its effectiveness in simulating concrete behavior under complex stress states [34]. Each node has three translational DOFs. This element is capable of performing nonlinear analysis, encompassing contact, large deformation, plasticity, and failure. Using solid C3D8R element, the studs and steel beam were modeled in one section and meshed together [35]. Based on the experimental constraints, the boundary conditions were set. Rigid constraints were applied to the bottom of the concrete slabs, as shown in Figure 5. The load on the specimen was applied as a concentrated force at the center of the steel girder but was coupled across the entire surface, thus simulated as a distributed load [36].

Furthermore, the steel stud is modeled using a bilinear isotropic hardening model, characterized by an initial linear elastic response followed by plastic deformation governed by a von Mises yield criterion. The contact interface between the steel stud and concrete is defined using a Coulomb friction model ensuring accurate simulation of potential sliding and separation at the interface. In addition, it should be mentioned that the analysis is conducted with geometric nonlinearity enabled, allowing for large deformation effects to be captured. This approach is crucial for accurately predicting the buckling and bending behavior of the steel stud under significant loads.

To expedite the analysis process, a coarse mesh was utilized to establish a general size. A mesh size study was carried out to evaluate the effect of mesh size on accuracy and time required for computation. Finer mesh sizes were employed at locations of maximum expected stresses to ensure the accuracy of the obtained results. The finest mesh was set on the stud and embedded in the surrounding concrete region. Their mesh sizes were the same. Where larger movements were expected, a finer mesh was set, such as on the loaded steel girder. For the concrete, we set a finer mesh at the site of the stud, extending to the

end of the stud. The endpoints of the finite elements along the stud, for both the concrete and the studs, converge at the same points. We were very careful to ensure that the mesh was completely symmetrical across the entire specimen. The overall mesh of the model consisted of approximately 680,000 elements. Figure 6 illustrates the specimen's FE mesh.

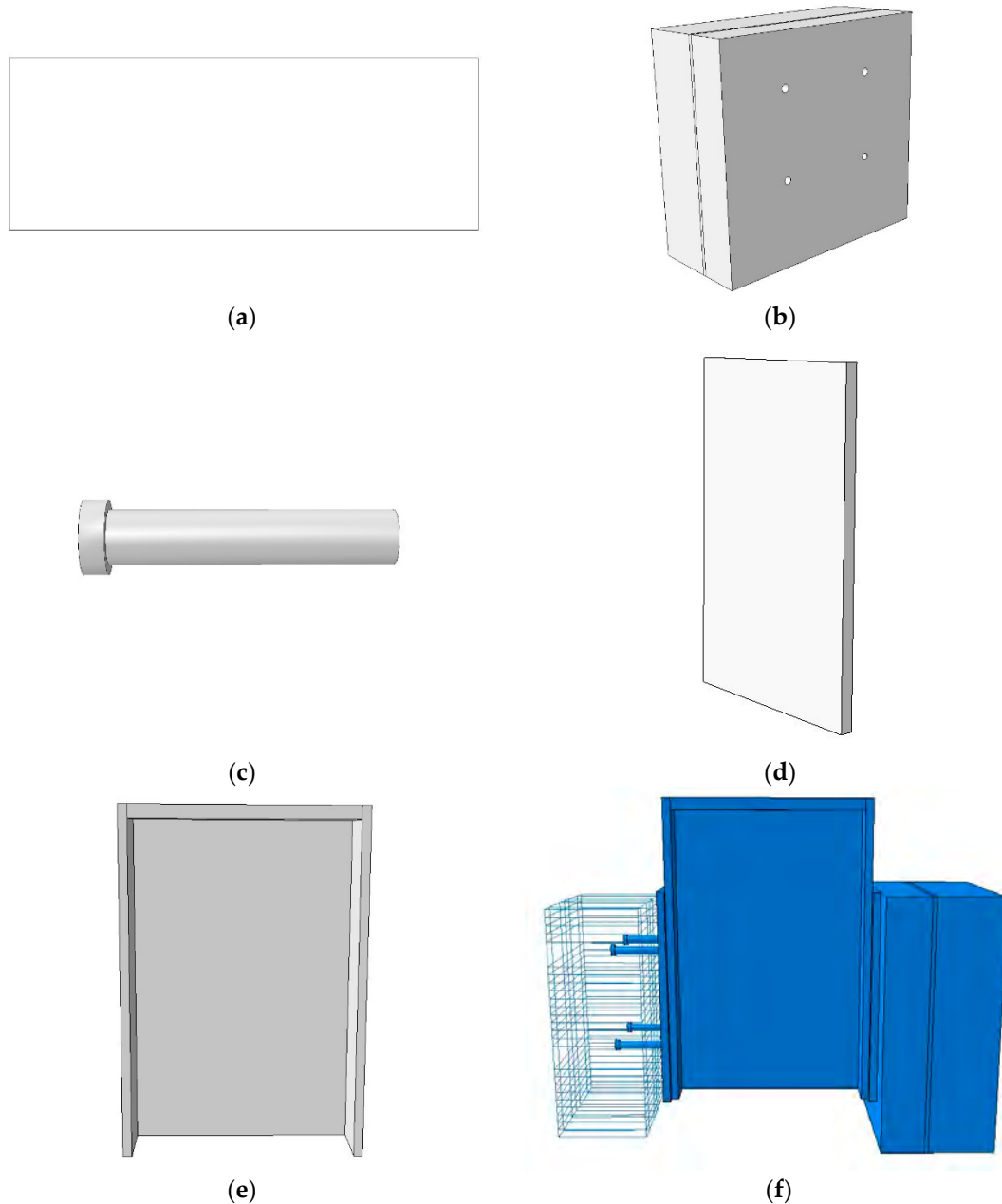


Figure 4. The considered FE model with its parts: (a) steel reinforcement bar; (b) concrete; (c) steel studs; (d) steel plate; (e) steel beam; (f) full model.

Accurate simulation of concrete material response under diverse loading conditions is essential in the modeling of concrete structures. To achieve this, the Concrete Damage Plasticity (CDP) model is frequently employed in finite element analysis. This model is particularly effective in capturing concrete nonlinear behavior, which is defined by both plastic deformation and damage under different stress states. The CDP model accounts for the two primary failure mechanisms in concrete: tensile cracking and compressive crushing. Tensile cracking occurs when the material's tensile strength is surpassed by the tensile stress, resulting in the formation of cracks. On the other hand, compressive crushing happens

when the compressive stress surpasses the concrete's compressive strength, causing the material to crush and fail.

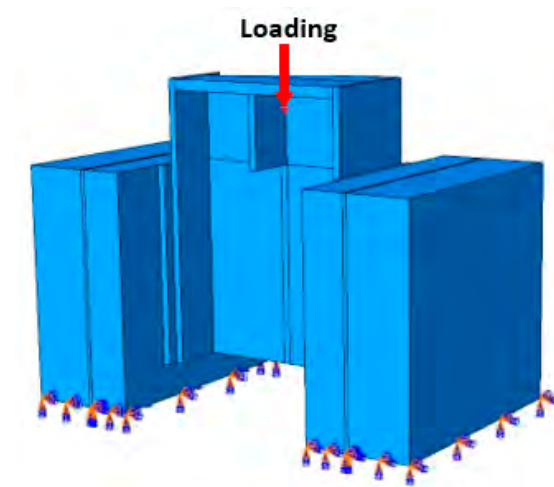


Figure 5. Boundary and loading condition of the model.

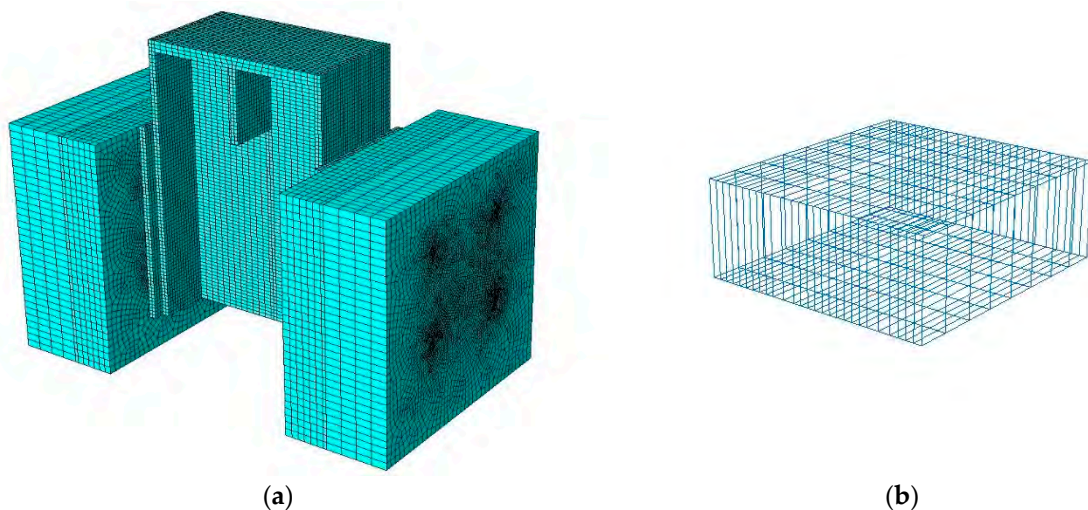


Figure 6. Details of the model's mesh: (a) Full model; (b) reinforcement cage.

The CDP model incorporates these failure mechanisms by combining plasticity and damage mechanics. The plasticity component of the model addresses the inelastic (plastic) strains that develop as the concrete undergoes irreversible deformation. This is based on a yield criterion that defines the transition from elastic to plastic behavior, often using yield surfaces adapted for concrete, such as the Drucker–Prager or Mohr–Coulomb criteria.

The CDP model's defining parameters such as the dilatancy angle, flow potential, damage variables, and strength ratios play a crucial role in defining concrete's failure envelope at various stress levels. By integrating these components, the CDP model enables a realistic simulation of concrete's response to complex loading conditions, including cyclic loading, which is essential for predicting the structural performance under service and ultimate load conditions.

To describe the behavior of concrete, the CDP plasticity model [37] requires some parameters, which are listed in Table 2.

Table 2. CDP input parameters for concrete.

Dilation Angle	Eccentricity	f_{b0}/f_{c0}	K
33	0.1	1.12	0.667

Particularly, the Poisson's ratio is defined as $\nu = 0.2$ and the Young's modulus of concrete is set at $E_0 = 35,000 \text{ N/mm}^2$. Tensile cracking and compressive crushing, which correspond to the failure modes shown in Figure 3, are included in the concrete damage plasticity data.

The components were carefully assembled and precisely positioned to construct the model depicted in Figure 4. Appropriate constraints were utilized to establish the interactions between the components. Figure 7a demonstrates the connection between the nodes on the concrete slab's surface and the studs by applying tie contact, ensuring that there is no relative slip between the surfaces.

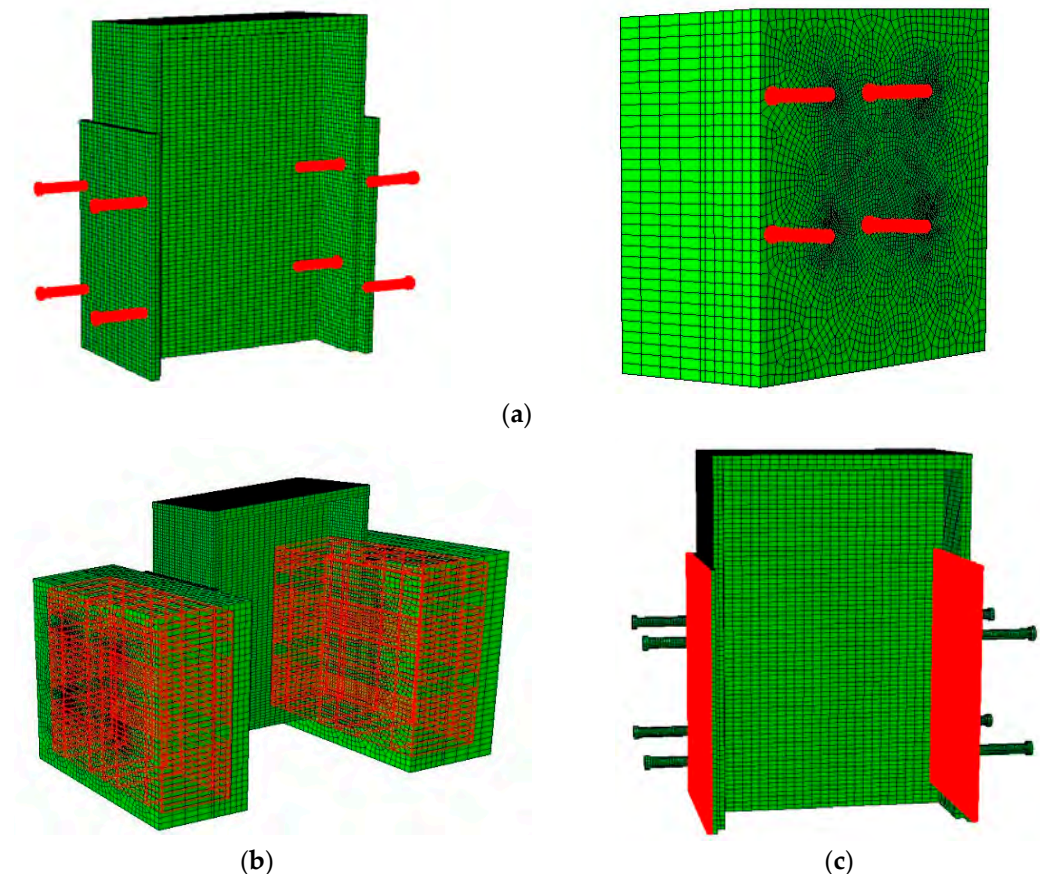


Figure 7. Considered constraints within the model. (a) Tie constraint surfaces between studs and concrete. (b) Embedded rebars in the concrete slab. (c) Contact surfaces between concrete and steel plates.

The steel and concrete surfaces depicted in Figure 7c were subjected at the beginning to frictionless contact interaction during the first step of the analysis. Rebars were incorporated into the concrete slab, as shown in Figure 7b, with embedded constraints applied to ensure their seamless integration with the slab. This limitation restricts the movement of the rebars' nodes to the calculated values of the concrete elements' degrees of freedom, without considering any slipping or debonding of the rebars.

4. Validation of Finite Element Model Based on Experimental Test

The purpose of validating the finite element model is to ensure that the numerical simulations accurately represent real-world conditions and to enhance the model's predictive capability. This validation process is essential for confirming that the numerical results reflect actual structural behavior, which is crucial for reliable analysis and design.

To achieve this, a comprehensive validation approach was adopted, incorporating detailed analytical investigations beyond mere verification. Initially, the comparison of

load–slip curves between the numerical model and experimental results was performed. This comparison revealed the significant impact of contact friction on the accuracy of the model. The initial model, assuming frictionless contact, showed discrepancies compared to experimental data, highlighting the need for incorporating friction elements to accurately simulate real conditions.

Furthermore, the friction coefficients used in the finite element model were derived from experimental test results. Once determined, these coefficients were kept constant throughout the simulation process. This decision was based on the assumption that the friction values were calibrated.

It should be acknowledged that the comparison is contingent upon a variety of parameters, particularly the presence or absence of contact friction parts. A load–slip curve per stud has been employed to facilitate the comparison of numerical and experimental results. The slip denotes the displacement exerted at the upper section of the girder, whereas the load signifies the resultant force derived from node forces generated by the FE model.

Prior to commencing the analysis of numerical and experimental data, it is essential to perform an initial calculation to demonstrate the significance of incorporating contact finite elements into the model. For this purpose, Figure 8 illustrates a comparison of two curves: the first one represents the numerical model assuming no friction between the studs and the concrete embedding slab and between the steel flange girder and the concrete slab. The second curve represents the experimental results. It seems that the numerical model with the assumption of frictionless contact is less resistant than what is observed in reality, which raises doubts about the hypothesis of displacement continuity.

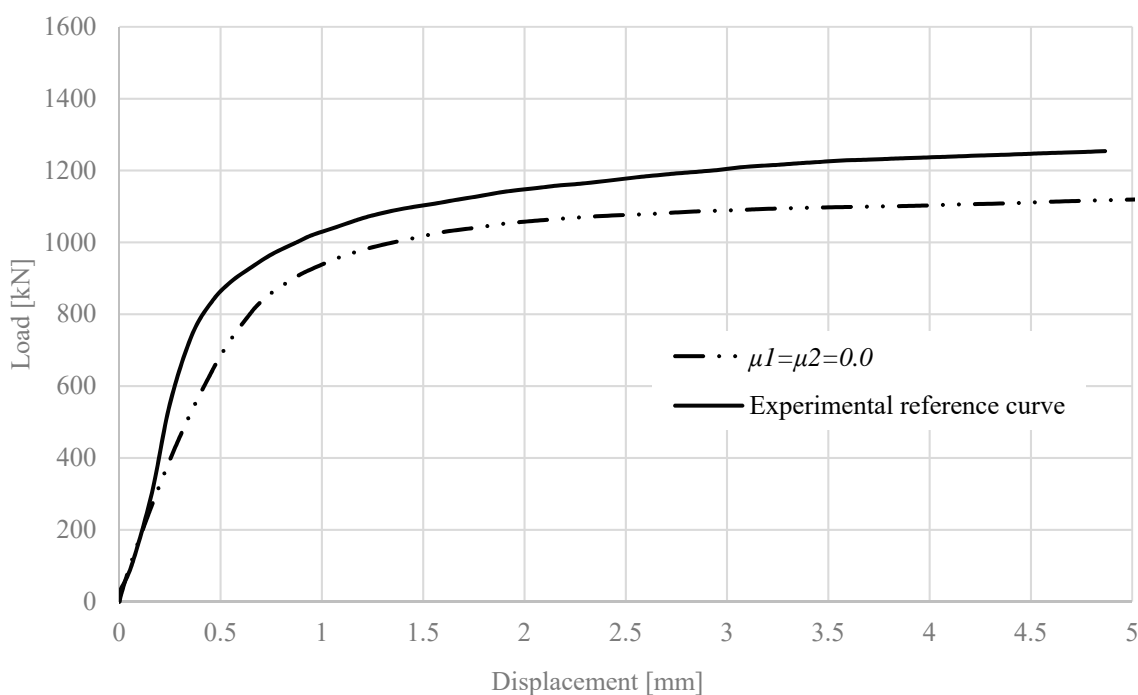


Figure 8. Experimental and frictionless FE model results.

After completing the frictionless contact numerical model, the second phase of the numerical analysis involves incorporating frictional contact between the concrete slab and the steel flange girder, as well as between the studs and the embedding concrete. For this investigation, the friction coefficients μ_1 between the steel flange girder and the concrete slab and μ_2 between the studs and the slab concrete are changing as shown in Table 3, assuming that $\mu_1 = \mu_2$. From the data presented in Figure 9, it is evident that the numerical solution achieved with $\mu_1 = \mu_2 = 0.2$ is more closely aligned with the experimental reference curve compared to the other values. It is important to mention that this technique yields an initial stud stiffness that is lower than the one estimated based on the testing data. This may

be attributed to the omission of considering the filling concrete's chemical bond friction during the first loading.

Table 3. Friction coefficient values.

Friction Coefficient			Value				
μ_1	0.0	0.1	0.2	0.3	0.4	0.5	
μ_2	0.0	0.1	0.2	0.3	0.4	0.5	

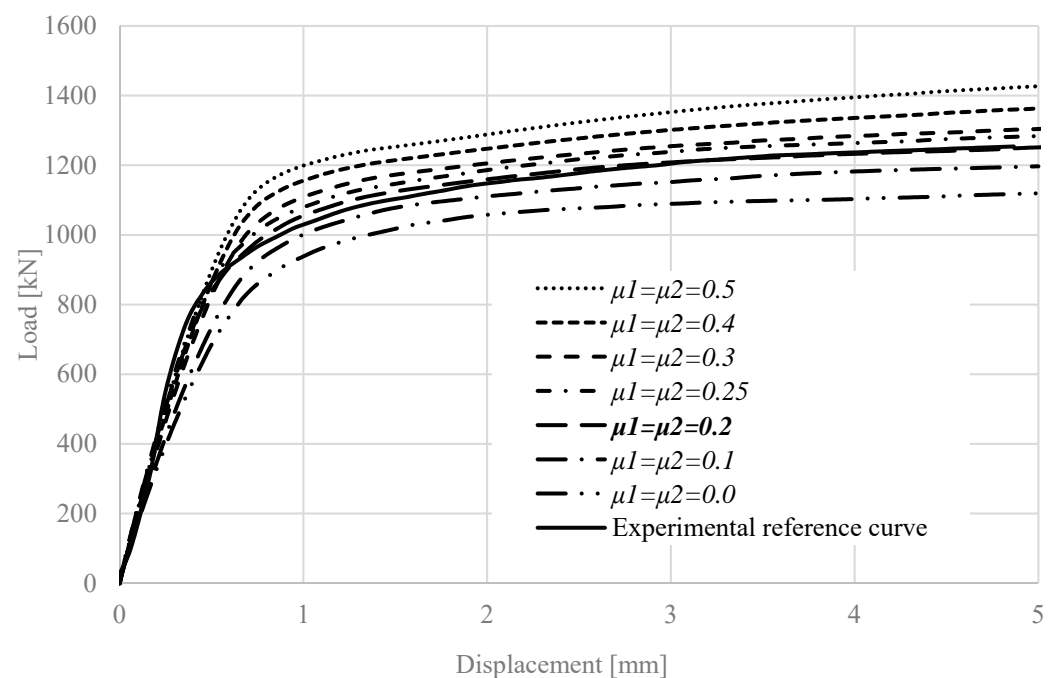


Figure 9. Experimental and FE model results.

The second calibration targets the friction coefficient (μ_1) between the steel flange girder and concrete slab. A series of μ_1 values—0.0, 0.1, 0.2, 0.3, 0.4, and 0.5—are tested. Meanwhile, the friction coefficient (μ_2) between the studs and the concrete slab is kept constant at 0.2. As shown in Figure 10, the numerical model with $\mu_1 = 0.2$ aligns most closely with the experimental reference curve, outperforming other values.

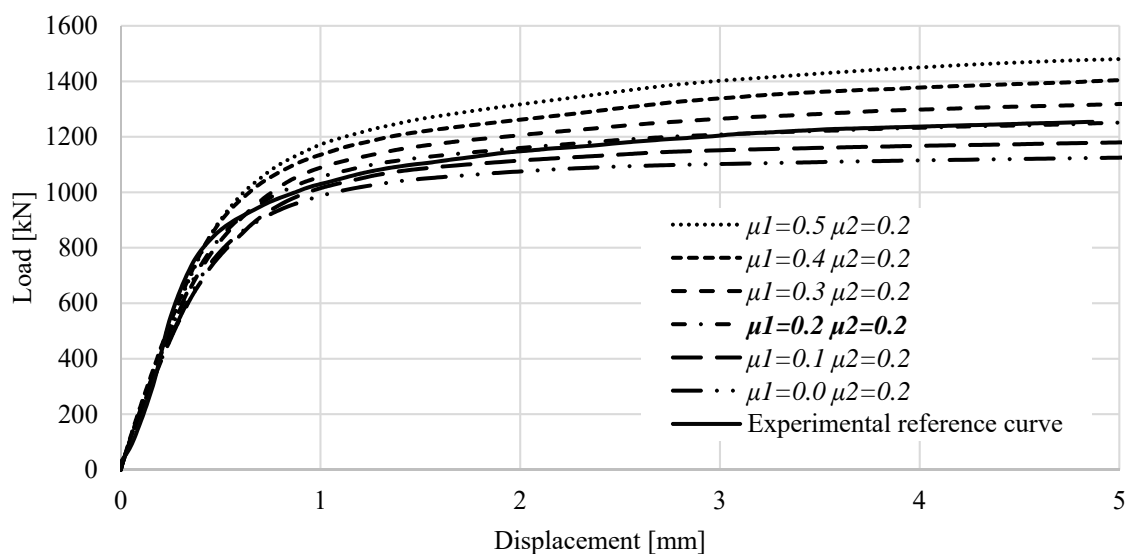


Figure 10. Influence of friction coefficient (μ_1), with $\mu_2 = 0.2$.

The third phase of calibration pertains to adjusting the friction coefficient μ_2 at the interface between the studs and the concrete. At this stage, μ_2 is allowed to vary, while the friction coefficient between the concrete and the girder flange, μ_1 , remains fixed at 0.2. As shown in Figure 11, the numerical model with $\mu_2 = 0.3$ provides the closest match, even exceeding the experimental reference curve. The comparison of the proposed model with experimental data yields positive results, enabling the fine-tuning of the friction coefficients μ_1 and μ_2 relevant to the push-out test. A friction coefficient of $\mu_1 = 0.2$ is applied to represent the interaction between the studs and the concrete, while $\mu_2 = 0.3$ is used to define the friction at the steel flange–concrete interface. Notably, the numerical model highlights that potential separation between steel and concrete, combined with friction at the girder flange–concrete interface, significantly impacts the results. Figure 11 further shows that the friction coefficient between the studs and the deck slab has a comparatively minor effect on the static behavior of the composite connection.

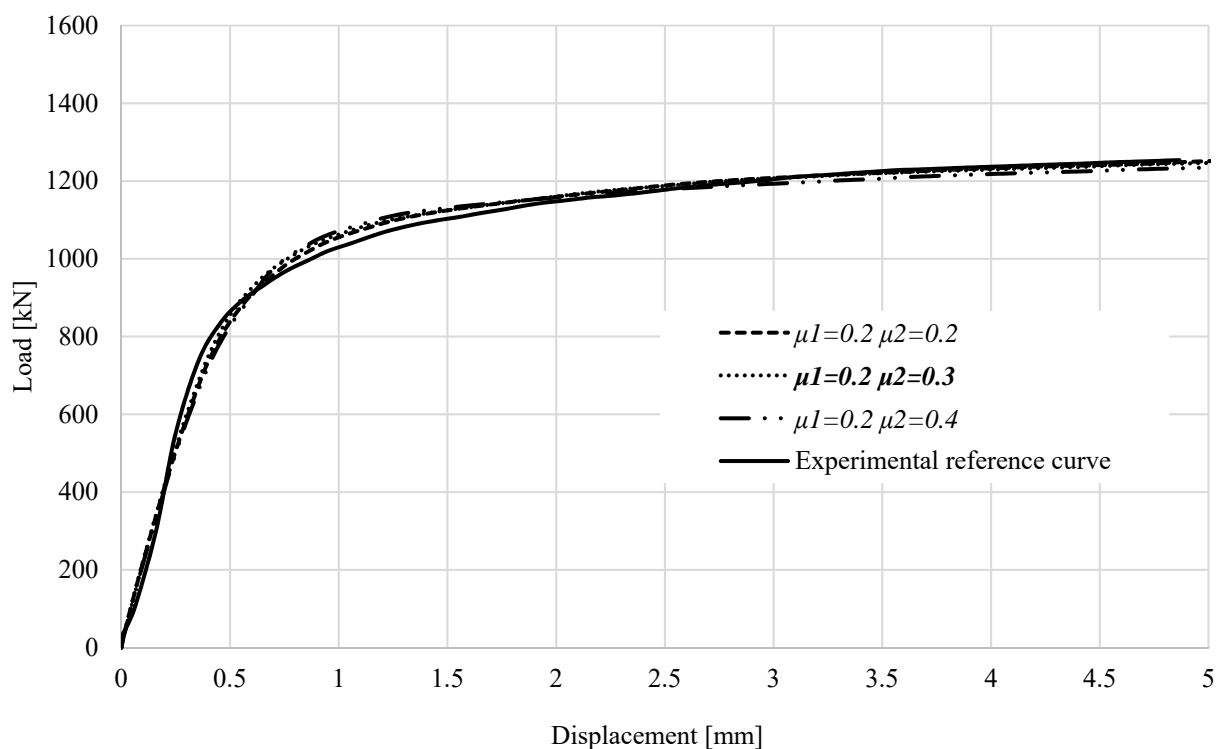


Figure 11. Influence of friction coefficient μ_2 , with $\mu_1 = 0.2$.

Beyond the comparison of load–displacement curves, it is beneficial to evaluate stresses and deformations in both the simulation and the actual model. ABAQUS enables the examination of any structural component at any load stage. Consequently, the validation of the numerical simulation can be accomplished by comparing the observed opening of studs in the experimental test specimens. Figure 12 represents the stress intensity obtained from numerical simulations for both the steel plate and the studs at the point of failure. Moreover, Figure 13 clearly shows the experimental and numerical deformed shapes of the stud. It should be mentioned that the upper section of the steel segment begins to undergo deformation while the remaining portion of the model maintains a more rigid panel-like structure.

It should be noted that the analysis is halted at the maximum load, prior to the onset of any softening behavior, as the focus of this study is on identifying the peak load capacity of the system. In this context, softening, such as post-peak concrete cracking or steel yielding leading to necking, is not captured. This is a deliberate choice, as the analysis aims to provide conservative estimates of structural performance under peak loading conditions.

Future work could extend this study by including softening models to explore post-peak responses and potential failure mechanisms.

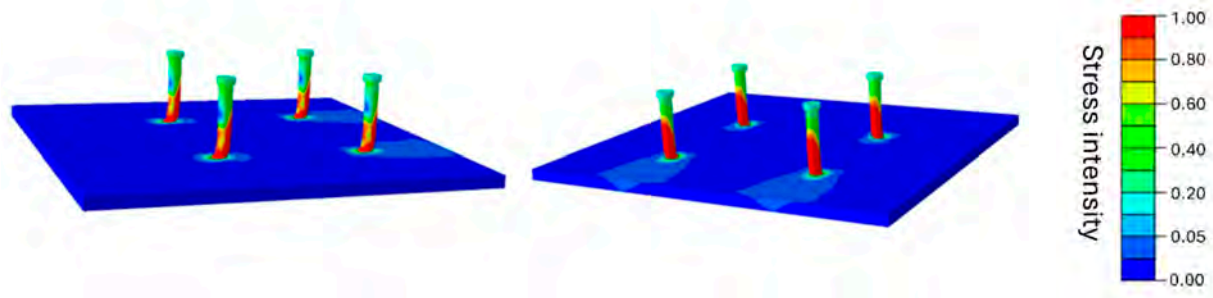


Figure 12. Steel plate and stud stress intensity.

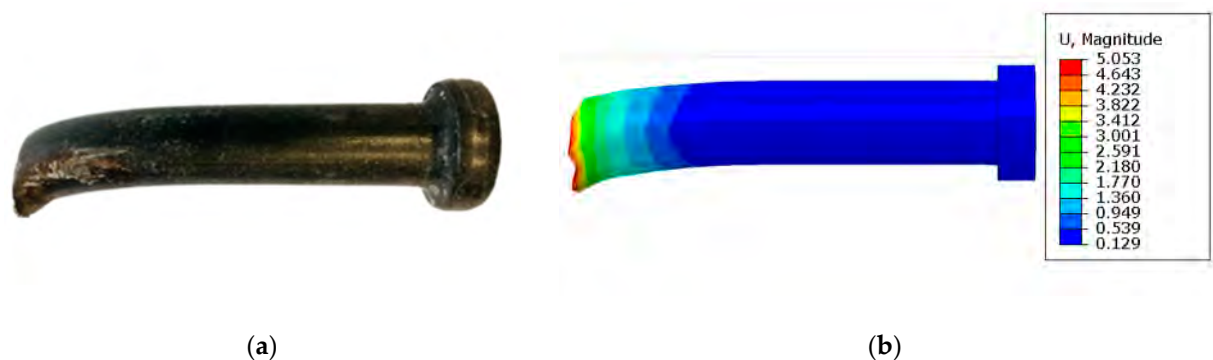


Figure 13. Deformed shapes of stud. (a) Experimental; (b) Numerical model.

Figure 14 illustrates the comparison of concrete damage, revealing identical damage zones in both the numerical model and the experiment with equal depth and extent. This comparison serves to confirm the validity of the model.

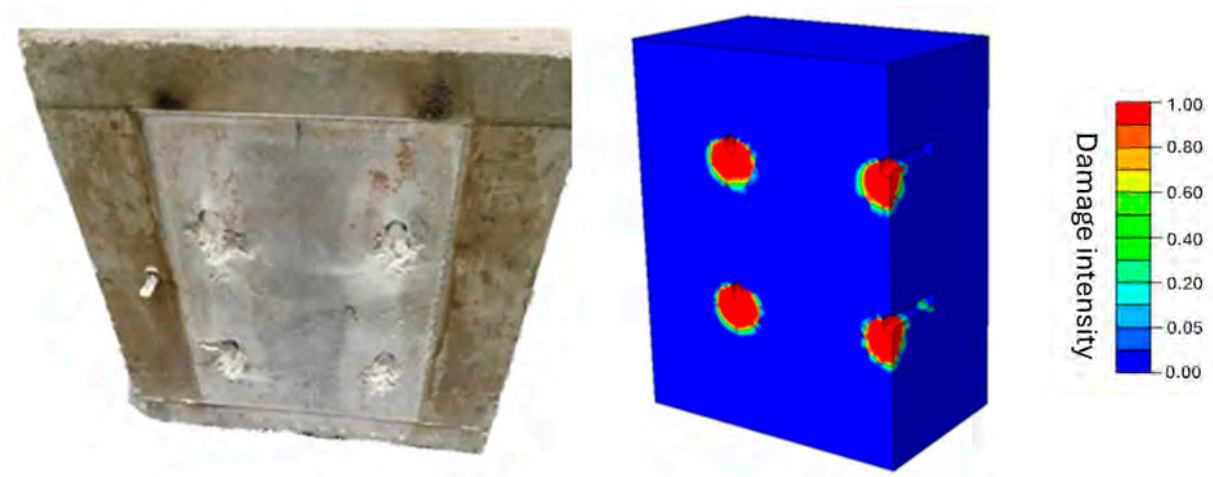


Figure 14. Concrete damage comparison.

5. Static Principle of Plastic Limit Analysis Used for Modelling

The static principle of plastic limit analysis is crucial for understanding the finite element (FE) numerical study presented in this work. This section provides a theoretical background on the static principle and its role in structural modeling.

Plastic limit analysis is a method used to determine the maximum load a structure can sustain before it experiences plastic collapse. In this context, “plastic collapse” refers to the condition where the structure undergoes irreversible deformation, leading to failure. The

method assumes that the material behaves according to plasticity theory, where it deforms elastically up to a certain stress level (the yield stress) and plastically beyond that.

The foundational formulation and proof of the static principle of limit analysis assumes a constant increasing force F_i is applied on the elasto-plastic body in the limit analysis [38]. This, one-parameter loading formula is shown below:

$$F_i = m F_0 \quad (1)$$

where m , a scalar parameter that increases monotonically, is the load multiplier, and F_0 is the predetermined external applied force. While m increases further and the area of the plastic regions grows during the load process, it is in a condition of unrestricted plastic flow m_p . This occurs when the plastic strains and displacements can be increased under constant external forces for the first time. When an elasto-plastic body experiences unlimited plastic deformation in one or more regions under constant external load, this is termed as the plastic limit state,

$$F_p = m_p F_0 \quad (2)$$

where F_p represents the body's plastic limit load, m_p denotes the plastic limit load multiplier and F_0 is the specified external applied force. In the plastic limit state, the equilibrium of the body is sustained by stresses and external forces across all conditions, thus necessitating the application of equilibrium equations. We consider a scenario wherein stress σ_{ij} within a body remains in quasi-static equilibrium with the plastic limit load, alongside another arbitrary stress σ_{ij}^s , which adheres to static permissibility conditions, and force $F_s = m_s F_0$, satisfying yield condition

$$f(\sigma_{ij}^s, k) \leq 0 \quad (3)$$

where k represents the plastic properties of the material of the body. In the context of a deformable body, as illustrated in Figure 15, the principle of virtual velocities may be extended to stress and force fields,

$$\int_V \sigma_{ij} \dot{\epsilon}_{ij} dV = m_p \int_{S_q} F_0 v_i dS \quad (4)$$

$$\int_V \sigma_{ij}^s \dot{\epsilon}_{ij} dV = m_s \int_{S_q} F_0 v_i dS \quad (5)$$

where $\dot{\epsilon}_{ij}$ represents strain rate, V denotes the volume of the deformable body, v_i signifies the velocities, and S_q represents the loading surface of the body.

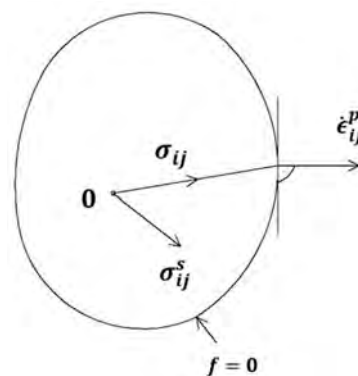


Figure 15. Body maintains a quasi-static equilibrium.

The two equations can be subtracted from each other, and the following equation is obtained.

$$\int_V (\sigma_{ij} - \sigma_{ij}^s) \dot{\epsilon}_{ij} dV = (m_p - m_s) \int_{S_q} F_0 v_i dS \quad (6)$$

Everywhere on the body, the convexity of the yield surface and normality can be employed:

$$(\sigma_{ij} - \sigma_{ij}^s) \dot{\epsilon}_{ij} \geq 0 \quad (7)$$

Based on the above equation, it can be deduced that

$$(m_p - m_s) \int_{S_q} F_0 v_i dS \geq 0 \quad (8)$$

In this equation, the integral signifies the work performed by external forces at the current velocities of the body. Drawing from the preceding equation, it can be inferred, within the context of the plastic limit state, that the work cannot exhibit negative values. Based on the static principle, load multiplier m_s is restricted to being less than or equal to plastic limit load multiplier m_p [39],

$$m_p - m_s \geq 0 \quad (9)$$

6. Deck Slab-Girder Connection Modelling with Concrete Slab under Compression

While traditional push-out tests typically do not involve compression, as discussed in previous sections, our experimental data were successfully validated against our numerical model, as demonstrated in Section 3. This model, therefore, provides a valuable opportunity for further exploration. Thus, this section focuses on investigating the role of friction when the concrete slab is under compression. Specifically, utilizing the presented model, various load cases were simulated to analyze the impact of the friction factor between different model components.

The design of steel–concrete bridges often neglects the consideration of compressive stresses acting on the bridge, such as self-weight, during the calculation of connections. Additionally, it fails to account for surface interaction and the friction coefficient. Numerical modeling enables the incorporation of these factors, providing a more accurate understanding of the behavior of connections and the overall structural performance. Conventional push-out tests, typically employed to assess shear connection strength, do not fully replicate the conditions experienced by real deck–slab connections. For instance, push-out tests generally lack the incorporation of compressive forces that are present in real structures due to self-weight, vehicle loads, and environmental effects. Moreover, they do not account for surface interactions and friction between the steel and concrete components under realistic loading conditions. These omissions can lead to an underestimation of the connection's load-carrying capacity in real-world applications. To make push-out tests more representative, modifications such as applying a consistent compressive force on the concrete slab and incorporating friction effects at the interface between the steel girder, concrete slab, and shear studs should be considered.

Two forces were employed in the modeling process: F_v , symbolizing a vertical load (normal compressive) imparted as compression onto the face of the concrete slab, and F_h , denoting a horizontal load applied to the face of the steel girder. The vertical load was uniformly distributed across the entire surface of the concrete. The modelling process comprised two steps. In the initial step, a static general analysis created the vertical load, while in the subsequent step, the vertical load was propagated, and a horizontal load was introduced through static riks analysis. That means F_v was constant load, which compressed the test specimen throughout the entire analysis, while F_h was incrementally increased until the load capacity was reached. This method closely follows real-life conditions and is well suited for practical applications. F_{h0} , with a value of 120 kN, was consistent with

the previous modelling. In the numerical modelling using ABAQUS, it is recommended to record approximately 10% of the initial load relative to the load capacity. This practice ensures that the solution maintains sufficient accuracy throughout the iterative process, thereby enabling a precise determination of the specimen's plastic load capacity. The vertical load (F_{v0}) was systematically varied in different model runs, encompassing range of values varying from 0 kN to 1800 kN.

The vertical loads simulate the conditions experienced by bridges under real-life scenarios, encompassing self-weight, vehicle loads, and other factors. The magnitudes of these forces are contingent on various parameters such as layer thickness, cross-section width, the number of vehicle lanes, and the number of main beams. Generally, forces within the range of approximately 200–1000 kN effectively represent these typical loads. All other modelling parameters remained consistent with those employed in the previous modelling.

Figure 16 represents the relative increase in the horizontal load. The horizontal axis illustrates the relative increase in horizontal load capacity compared to the situation without a vertical load $F_{v0} = 0$ kN. As the initial compression load increases, it is evident that the force-displacement performance of the connection also increases. This discrepancy in load capacity between standard push-out test results and real deck–slab connections is notable. While the standard push-out test is inherently biased toward safety, practical connections exhibit significantly higher load capacity. The results presented in Figure 16 highlight the substantial impact of incorporating the friction coefficient between components of composite connections and modelling real load cases in the analysis. The self-weight of structural elements above the main girders, along with additional loads such as vehicles, enhances safety by counteracting various magnitudes of horizontal forces resulting from friction between the concrete deck slab and the steel girder, and additionally between the concrete deck slab and the studs.

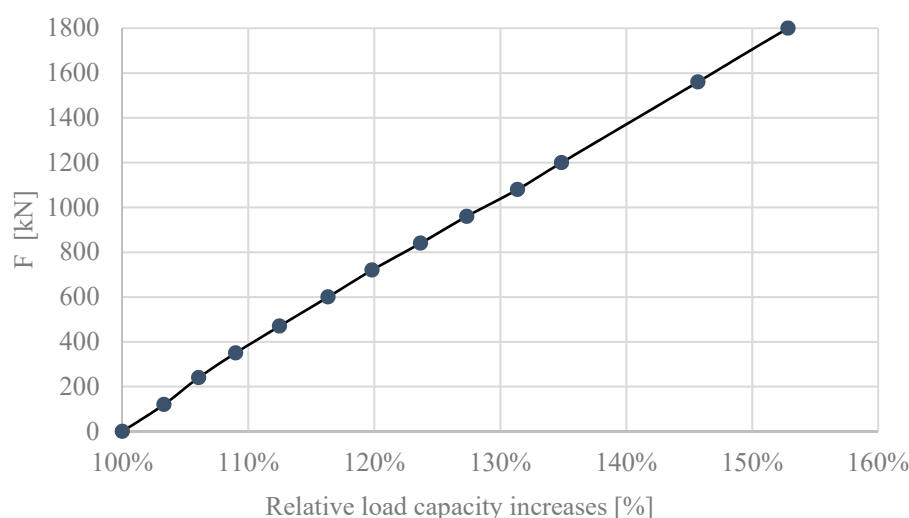

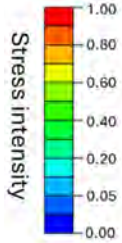
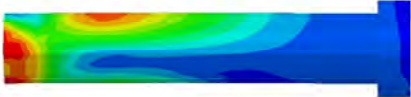
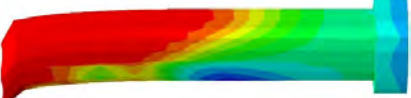

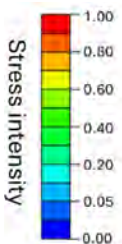

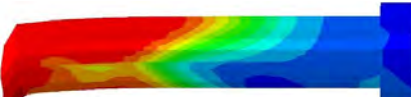

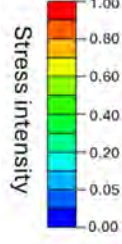

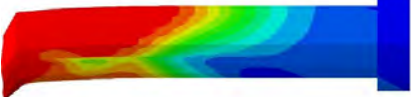

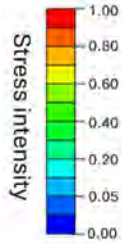

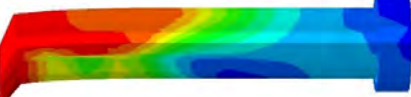


Figure 16. Relative horizontal load capacity increases.

To further analyze the structural behavior, plastic-limit analysis principles were applied and multiple simulations were conducted in ABAQUS, each corresponding to a specific value of the static load multiplier (m_s) including the plastic-limit load multiplier (m_p). Table 4 represents the stress intensity experienced by studs at the point of failure in different load cases. The application of plastic-limit analysis allowed us to capture the nonlinear behavior of the connection and understand how it behaves under extreme loading scenarios. The results demonstrate the significance of vertically loaded conditions in influencing stress distribution and failure patterns, which has implications for structural design and assessment.

Table 4. Stud stress intensity in different load cases.

m_s	m_p	Vertical Load	Stresses in Stud	Stress Intensity (σ/σ_y)
2.11	5.45	$F_v = 0 \text{ kN}$		
2.82				
5.45				
2.67	5.94	$F_v = 360 \text{ kN}$		
3.65				
5.94				
3.13	6.53	$F_v = 720 \text{ kN}$		
4.22				
6.53				
3.73	7.35	$F_v = 1200 \text{ kN}$		
5.03				
7.35				

The observed variations in stress distribution across the studs offer valuable insights into the failure mechanisms inherent in composite steel–concrete connections. Under horizontal loaded conditions, extensive failure was observed extending to the length of the stud. In contrast, for other load cases, failure was more localized and occurred primarily at the connection between the steel plate and the stud. This observation underscores the importance of considering the connection details and interface properties in structural analysis and design.

Furthermore, the deviation from traditional push-out test expectations highlights the complex nature of failure mechanisms in real-world bridge applications. By elucidating the stress distribution and failure patterns, the proposed work provides valuable insights into enhancing the resilience of composite steel–concrete connections against various loading scenarios.

The detailed analysis of stress distribution and failure mechanisms, coupled with the application of plastic-limit analysis principles, contributes to a comprehensive understanding of the structural behavior of composite steel–concrete connections. These findings pave the way for informed design decisions and facilitate the development of resilient and efficient bridge structures.

7. Conclusions

The validation process of the proposed model against experimental data yielded favorable outcomes and facilitated the adjustment of friction coefficients μ_1 and μ_2 pertinent to the push-out test. A friction coefficient value of $\mu_1 = 0.2$ was employed to characterize the interaction between the studs and the concrete, whereas $\mu_2 = 0.3$ was chosen to represent the friction between the steel flange and the concrete slab. Significantly, the impact of the friction between the concrete and the flange of the girder on the numerical outcomes was observed to be substantial.

The experimental result was successfully used to validate the finite element (FE) model. Validating the model entails comparing the stresses and deformations observed in the simulation to those in the real model. ABAQUS enables the examination of any stage of the increments, allowing for a comprehensive comparison. The numerical simulation is validated by assessing stresses, deformations, and concrete damages, ensuring consistency between the model and experimental observations.

The proposed work uncovered notable disparities in the horizontal load-displacement behavior between conventional push-out tests and real-world deck–slab connections. While conventional tests prioritize safety margins, this work underscored the increase in the plastic reserves, load capacity, and horizontal force-displacement performance which are exhibited by practical connections. Furthermore, variations in the stress distribution of the studs under different loading scenarios were observed, with compression leading to more localized failures at the joints.

In the case of no compression, extensive failure with pronounced deformations extending to the center of the stud was observed. Conversely, when compression is applied, the failure becomes more concentrated and is located at the joint. Additionally, stresses and deformations along the studs are smaller compared to the previous case.

The self-weight of the structural elements the steel structure, combined with additional loads, contributes to the safety of the system by mitigating the effects of varying magnitudes of horizontal forces resulting from friction between connection components.

In practical terms, the proposed work in this research offers valuable insights for the design and implementation of steel–concrete composite structures. By emphasizing the intricate aspects of structural behavior and the inherent limitations of traditional testing methodologies, this research advocates for a refined approach to structural analysis and design. These insights emphasize the need for advanced predictive models and suggest the potential for revisions to existing design codes and construction practices. The improved understanding of stress distribution, load-bearing capacities, and plastic reserves highlighted in this study could inform future regulations, ensuring more accurate and

efficient designs of composite structures. Furthermore, the findings from this study may guide the development of new construction techniques that better account for the nuanced interactions between materials under various loading conditions.

Author Contributions: D.G.: Writing—Original Draft, Investigation, Visualization, R.C.: Supervision, Validation, Software, J.S.: Investigation, Resources, Data Curation, M.D.: Conceptualization, Validation, Software, O.G.: Writing—Review and Editing, Methodology, M.M.R.: Software, Writing—Review and Editing, Supervision. All authors have read and agreed to the published version of the manuscript.

Funding: This research received no external funding.

Data Availability Statement: The data presented in this study are available upon corroborated request from the corresponding author.

Acknowledgments: The authors acknowledge the support of those who directly or indirectly contributed to the success of this study.

Conflicts of Interest: The authors declare no conflict of interest.

References

1. Roš, M. Les constructions acier-beton system Alpha. *L'Ossature Métallique* **1934**, *4*, 195–208.
2. Newmark, N.M.; Siess, C.P.; Viest, I.M. Tests and analyses of composite beams with incomplete interaction. *Soc. Exp. Stress Anal.* **1951**, *9*, 75–92.
3. Viest, I.M. Investigation of stud shear connectors for composite concrete and steel T-beams. *J. Am. Concr. Inst.* **1956**, *27*, 875–891.
4. Thurlimann, B. Fatigue and static strength of stud shear connectors. *J. Proc.* **1959**, *55*, 1287–1302.
5. Abambres, M.; He, J. Shear Capacity of Headed Studs in Steel-Concrete Structures: Analytical Prediction via Soft Computing. *IUP J. Struct. Eng.* **2020**, *XIII*, 40–64. [\[CrossRef\]](#)
6. Slutter, R.G.; Driscoll, G.C. Flexural strength of steel-concrete composite beams. *J. Struct. Div. (ASCE)* **1965**, *91*, 71–99. [\[CrossRef\]](#)
7. Mainstone, R.J.; Menzies, J.B. Shear connectors in steel-concrete composite beams for bridges. *Concrete* **1967**, *1*, 291–302.
8. Oehlers, D.J.; Coughlan, C.G. The shear stiffness of stud shear connections in composite beams. *J. Constr. Steel Res.* **1986**, *6*, 273–284. [\[CrossRef\]](#)
9. EN 1994-1-1:2004; Eurocode 4: Design of Composite and Concrete Structures—Part 1-1: General Rules and Rules for Buildings. European Committee for Standardization: Brussels, Belgium, 2004.
10. Psota, J.; Rotter, T. New conception of the shear connector for composite bridge decks. *Procedia Eng.* **2012**, *40*, 387–392. [\[CrossRef\]](#)
11. Lacki, P.; Derlatka, A.; Kasza, P.; Gao, S. Numerical study of steel-concrete composite beam with composite dowels connectors. *Comput. Struct.* **2021**, *255*, 106618. [\[CrossRef\]](#)
12. Hällmark, R.; Collin, P.; Hicks, S.J. Push-out tests of coiled pins vs. headed studs. *J. Constr. Steel Res.* **2019**, *161*, 1–16. [\[CrossRef\]](#)
13. Luciano, M.B.; Wallison, C.S.B.; Jorge, B.; Otávio, R.O.C. Truss-type shear connector for composite steel-concrete beams. *Constr. Build. Mater.* **2018**, *167*, 757–767.
14. Berthelmy, J. Fatigue designed CL-cutting shape: A new economic steel-concrete connection system and some applications for bridges. *Procedia Eng.* **2013**, *66*, 138–149. [\[CrossRef\]](#)
15. Brozzetti, J. Design development of steel-concrete composite bridges in France. *J. Constr. Steel Res.* **2000**, *55*, 229–243. [\[CrossRef\]](#)
16. Kim, S.-H.; Choi, J.; Park, S.-J.; Ahn, J.-H.; Jung, C.-Y. Behavior of composite girder with Y-type perfobond rib shear connectors. *J. Constr. Steel Res.* **2014**, *103*, 275–289. [\[CrossRef\]](#)
17. Cao, P.; Hu, X.; Liu, E.; Chen, J.; Jiang, S.; Ding, H. Research on Mechanical Behavior of the Steel–Concrete–Steel Composite Structures Subjected to High Temperature of Fire. *Materials* **2022**, *15*, 4872. [\[CrossRef\]](#)
18. Qiang, Z.; Yaozhuang, L.; Kolozvari, K. Numerical modeling of steel–concrete composite structures. *Struct. Concr.* **2018**, *19*, 1727–1739. [\[CrossRef\]](#)
19. Oguejiofor, E.C.; Hosain, M.U. Behaviour of perfobond rib shear connectors in composite beams: Full-size tests. *Can. J. Civ. Eng.* **1992**, *19*, 224–235. [\[CrossRef\]](#)
20. Rad, M.M.; Ibrahim, S.K.; Lógó, J. Limit design of reinforced concrete haunched beams by the control of the residual plastic deformation. In *Structures*; Elsevier: Amsterdam, The Netherlands, 2022; Volume 39, pp. 987–996. [\[CrossRef\]](#)
21. Szép, J.; Habashneh, M.; Lógó, J.; Movahedi Rad, M. Reliability Assessment of Reinforced Concrete Beams under Elevated Temperatures: A Probabilistic Approach Using Finite Element and Physical Models. *Sustainability* **2023**, *15*, 6077. [\[CrossRef\]](#)
22. Oguejiofor, E.C.; Hosain, M.U. A parametric study of perfobond rib shear connectors. *Can. J. Civ. Eng.* **1994**, *21*, 614–625. [\[CrossRef\]](#)
23. Oguejiofor, E.C.; Hosain, M.U. Numerical analysis of push-out specimens with perfobond rib connectors. *Comput. Struct.* **1997**, *62*, 617–624. [\[CrossRef\]](#)
24. Jayas, B.S.; Hosain, M.U. Behaviour of headed studs in composite beams: Push-out tests. *Can. J. Civ. Eng.* **1987**, *15*, 240–253. [\[CrossRef\]](#)

25. Kim, B.; Wright, H.D.; Cairns, R. The behaviour of through-deck welded shear connectors: An experimental and numerical study. *J. Constr. Steel Res.* **2001**, *57*, 1359–1380. [[CrossRef](#)]
26. El-lobody, E.; Young, B. Performance of shear connection in composite beams with profiled steel sheeting. *J. Constr. Steel Res.* **2006**, *62*, 682–694. [[CrossRef](#)]
27. El-lobody, E.; Lam, D. Modelling of headed stud in steel-precast composite beams. *Steel Compos. Struct.* **2002**, *2*, 355–378. [[CrossRef](#)]
28. Nguyen, H.T.; Kim, S.E. Finite element modelling of push-out tests for large stud shear connectors. *J. Constr. Steel Res.* **2009**, *65*, 1909–1920. [[CrossRef](#)]
29. Mirza, O.; Uy, B. Effects of the combination of axial and shear loading on the behaviour of headed stud steel anchors. *Eng. Struct.* **2010**, *32*, 93–105. [[CrossRef](#)]
30. Karalar, M.; Dicleli, M. Effect of pile orientation on the fatigue performance of jointless bridge H-piles subjected to cyclic flexural strains. *Eng. Struct.* **2023**, *276*, 115385. [[CrossRef](#)]
31. Karalar, M.; Dicleli, M. Low-cycle fatigue in steel H-piles of integral bridges; a comparative study of experimental testing and finite element simulation. *Steel Compos. Struct. Int. J.* **2020**, *34*, 35–51.
32. Guezouli, S.; Lachal, A. Numerical analysis of frictional contact effects in push-out tests. *Eng. Struct.* **2012**, *40*, 39–50. [[CrossRef](#)]
33. Rabbat, B.G.; Asce, M.; Russel, H.G. Friction coefficient of steel on concrete or grout. *J. Struct. Eng.* **1985**, *111*, 505–515. [[CrossRef](#)]
34. Bergan, P.G.; Holand, I. Nonlinear finite element analysis of concrete structures. *Comput. Methods Appl. Mech. Eng.* **1979**, *17*, 443–467. [[CrossRef](#)]
35. Colajanni, P.; La Mendola, L.; Latour, M.; Monaco, A.; Rizzano, G. FEM analysis of push-out test response of Hybrid Steel Trussed Concrete Beams (HSTCBs). *J. Constr. Steel Res.* **2015**, *111*, 88–102. [[CrossRef](#)]
36. Cheng, Z.Q.; Liu, H.; Tan, W. Advanced computational modelling of composite materials. *Eng. Fract. Mech.* **2024**, *305*, 110120. [[CrossRef](#)]
37. Khaleel Ibrahim, S.; Movahedi Rad, M. Limited Optimal Plastic Behavior of RC Beams Strengthened by Carbon Fiber Polymers Using Reliability-Based Design. *Polymers* **2023**, *15*, 569. [[CrossRef](#)] [[PubMed](#)]
38. Movahedi, R.M.; Lógó, J. Plastic behaviour and stability constraints in the reliability based shakedown analysis and optimal design of skeletal structures. *Eng. Mater. Sci.* **2011**, *93*, 203.
39. Movahedi Rad, M.; Habashneh, M.; Lógó, J. Elasto-Plastic limit analysis of reliability based geometrically nonlinear bi-directional evolutionary topology optimization. *Structures* **2021**, *34*, 1720–1733. [[CrossRef](#)]

Disclaimer/Publisher's Note: The statements, opinions and data contained in all publications are solely those of the individual author(s) and contributor(s) and not of MDPI and/or the editor(s). MDPI and/or the editor(s) disclaim responsibility for any injury to people or property resulting from any ideas, methods, instructions or products referred to in the content.